Biochimica et Biophysica Acta 1828 (2013) 1284–1292

Contents lists available at SciVerse ScienceDirect

Biochimica et Biophysica Acta

journal homepage: www.elsevier.com/locate/bbamem

Molecular origin of VDAC selectivity towards inorganic ions: A combined molecular and Brownian dynamics study

Eva-Maria Krammer, Fabrice Homblé, Martine Prévost *

Structure et Fonction des Membranes Biologiques, Centre de Biologie Structurale et de Bioinformatique, Université Libre de Bruxelles (ULB), Boulevard du Triomphe CP 206/2, B-1050 Brussels, Belgium

ARTICLE INFO

Article history:
Received 21 June 2012
Received in revised form 14 December 2012
Accepted 31 December 2012
Available online 9 January 2013

Keywords:
VDAC
Nanopore
Ion channel
Electrophysiology
Molecular dynamics
Brownian dynamics

ABSTRACT

The voltage-dependent anion channel (VDAC) serves as the major pore for metabolites and electrolytes in the outer mitochondrial membrane. To refine our understanding of ion permeation through this channel we performed an extensive Brownian (BD) and molecular dynamics (MD) study on the mouse VDAC isoform 1 wild-type and mutants (K20E, D30K, K61E, E158K and K252E). The selectivity and the conductance of the wild-type and of the variant channels computed from the BD trajectories are in agreement with experimental data. The calculated selectivity is shown to be very sensitive to slight conformational changes which may have some bearing on the variability of the selectivity values measured on the VDAC open state. The MD and BD free energy profiles of the ion permeation suggest that the pore region comprising the N-terminal helix and the barrel band encircling it predominantly controls the ion transport across the channel. The overall 12 μs BD and 0.9 μs MD trajectories of the mouse VDAC isoform 1 wild-type and mutants feature no distinct pathways for ion diffusion and no long-lived ion–protein interactions. The dependence of ion distribution in the wild-type channel with the salt concentration can be explained by an ionic screening of the permanent charges of the protein arising from the pore. Altogether these results bolster the role of electrostatic features of the pore as the main determinant of VDAC selectivity towards inorganic anions.

1. Introduction

The voltage-dependent anion channel (VDAC) is the major pore of the outer mitochondrial membrane. As a major pathway for solute translocation, VDAC plays a central role in energy production [1]. There is also growing evidence that VDAC is involved in calcium and apoptotic signaling though its precise role remains enigmatic [2–4]. Moreover, VDAC participates in important pathologies like cancer [5–7].

The regulation and function of VDAC can differ depending on the studied organism and the isoform type ([8,9] and references therein). All organisms with mitochondria have at least one isoform in common with similar electrophysiological properties (viz., conductance, voltage-dependence and selectivity) [10–12]. The physiological significance of this canonical isoform in the mitochondrial metabolism was suggested to be strongly correlated to its voltage-dependence [13]: at voltages close to 0 mV, the channel exists in a fully open state whereas upon higher voltages it switches to partially closed states. VDAC open state is characterized by a high conductance compatible with the magnitude of the metabolite flow through mitochondria and bya slight preference for inorganic anions over cations. [10,11]. In contrast, in its closed states, VDAC is no longer permeable to metabolites and shows a lower conductance for small ions with a preference for cations [1,10,11,14]. The open state of VDAC from various species including plants, animals and fungi features a similar selectivity and conductance [1,15–28]. Its selectivity has also been shown to be sensitive to several factors such as the ionic strength in yeast and plant [18,25,29], the lipid composition in plant [30] and to the introduction of single point mutations in yeast [17,18].

Three experimental 3D structures determined by X-ray crystallography and/or NMR of recombinant mouse (mVDAC1) and human VDAC isoform 1 (hVDAC1) refolded from inclusion bodies reveal a large pore formed by 19 antiparallel β-strands closed by two parallel strands [31–33]. In contrast to earlier structural models [34–36], in which the N-terminal region (residues 1 to 20) was proposed to be part of the barrel or to lie outside the barrel, all three 3D structures agree on the location of this segment inside the pore. These structures diverge however on the exact position of the N-terminal region, on its local structure and on its interactions with the barrel [31–33]. For the sake of clarity, the three experimental structures will be referred to as wild-type (wt) structures hereafter.

Abbreviations: BD, Brownian dynamics; hVDAC1, human VDAC isoform 1; MD, molecular dynamics; mVDAC1, mouse VDAC isoform 1; NMR3, hVDAC1 NMR structure conformation #3; N_{Cl^-}, time-averaged number of chloride; N_{K^+}, time-averaged number of potassium; PNP, Poisson–Nernst–Planck; RMSD, root-mean square derivation; RMSF, root-mean square fluctuation; yVDAC, yeast VDAC; ΔV_{rev}, difference between experimental and calculated average reversal potential values

* Corresponding author. Tel.: +32 2 6502049; fax: +32 2 6505382.
E-mail address: mprevost@ulb.ac.be (M. Prévost).

0005-2736/$ – see front matter © 2013 Elsevier B.V. All rights reserved.
http://dx.doi.org/10.1016/j.bbamem.2012.12.018

As some biochemical and functional data were reported to be at odds with these structures their biological significance has been questioned [35,37]. Since the proteins were refolded from inclusion bodies, it was proposed that the 3D structures might not be in the native conformation [35]. However these 3D structures are coherent with data reported in previous structural and bioinformatic studies of VDAC channels purified from fungi, plants and mammals [8,38–42]. Other reports examined the 3D structures in the light of electrophysiological data obtained in planar lipid bilayer and concluded that these data correlateswell with the 3D structures [43,44]. Several theoretical studies also demonstrated that these structures are anion selective like the VDAC open state [29,45–48]. That might not be enough to corroborate these structures. Further studies should be thus carried out show whether the recombinant protein is either in the nativeor in some other conformational state. The present work is in line with this strategy.

The study of these high-resolution structures, which are assumed to represent the open state of VDAC, with computer modeling and simulation tools gives the opportunity of unraveling the fundamental principles of ion translocation through the channel in atomic detail. Recent theoretical studies were carried out to get insight into the selectivity of mVDAC1 [48] and hVDAC1 [45,47] using two approaches: Poisson–Nernst–Planck (PNP) and Brownian dynamics (BD), respectively. Detailed all-atom molecular dynamics (MD) simulations were also performed to study the importance of the residue E73 for the dynamics of mVDAC1 [49] and to investigate the conductance and selectivity of the hVDAC1 structure [46]. Moreover, a combined MD simulation and continuum electrostatics study examined the salt concentration dependence of mVDAC1 selectivity [29].

Although these studies showed a preference of all three experimental structures for chloride over potassium regardless of the approach used [29,45–48] discrepancies arise in particular on the mechanism of selectivity. For example, in the study of hVDAC1 [46] the selectivity was reported to partially arise from interactions between K^+ and a few protein residues hindering thereby the translocation of cations relative to anions. Such interactions were not observed in the mVDAC1 MD study [29]. These discrepancies might originate either from structural differences between the two 3D structures and/or from the approximations inherent to the different modeling techniques. The fact that a significant variability in the selectivity computed by BD was observed for the 20 hVDAC1 NMR conformations [45] gives some support to the impact of conformational disparities.

To address the issue of the origin of selectivity and conductance in mVDAC1 wt and mutant proteins we resorted mainly to two theoretical approaches, namely MD and BD. The latter approach has the clear advantage over MD to be many orders of magnitude faster. It thus permits to rapidly calculate current–voltage (I/V) curves which can be directly compared to the physiological measurements. This approach was successfully applied to the study of several β-barrel channels [45,47,50,51]. The all-atom MD method offers a level of structural and dynamic atomic details that is essential to grab some of the features of ion permeation.

In the work presented here, MD and BD simulations were performed to study ion permeation across mVDAC1 structure. The salt concentration dependent variation of the distribution of ions inside the channel determined from BD matches remarkably well with that previously obtained in a MD study [29]. According to our BD simulations, the mVDAC1 structure seems to be slightly more anion-selective than the other two hVDAC1 structures [45,47]. To ascertain whether the encountered deviation ensues from structural differences among the experimental structures we investigated the impact of conformational changes on the selectivity computed by BD on snapshots of a MD trajectory generated from the crystal mVDAC1 structure.

Several experimental studies have revealed that the selectivity of yeast VDAC1 (yVDAC1) can be altered by the substitution of single charged residues inside the channel [17,18,25]. We thus selected 5 substitutions of charged residues among the yVDAC1 mutants whose selectivity was measured and that are conserved between yeast and mammals, namely K20E, D30K, K61E, E158K and K252E (numbering refers to mammalian sequences). The first three mutants feature a significant change in selectivity whereas E158K and K252E alter the selectivity of the channel in a negligible way [17,18]. We then investigated by BD and MD the transport of ions through these mVDAC1 mutants to refine our understanding of the molecular determinants governing ion translocation across molecular pores. Our simulations indicate that ion electrodiffusion is mainly guided by the distribution of fixed charges in the channel and point to a particular region in the pore that plays a significant role in the selectivity mechanism.

2. Material and methods

2.1. Molecular dynamics simulations

A preexisting equilibrated MD system of mVDAC1 (PDB ID: 3EMN [31]) embedded in POPE and in the presence of 0.1 M KCl (for more details see [29]) was used as a starting point for simulating the wt and mutant (K20E, D30K, K61E, E158K and K252E) protein. After addition of another 0.1 M KCl, the system was equilibrated for 12.5 ns using the following sequence: 2.5 ns with all protein atoms fixed, 2.5 ns with all backbone atoms fixed, and 7.5 ns with no restrained atoms. All simulations were carried out using the NAMD program [52] as described elsewhere [29]. For each system a 150 ns trajectory was produced. The production of such a trajectory took about 21 days using 64 cpus of our in house cluster (Quad-Core 2.3 GHz AMD Opteron Processors). The single mutant proteins were generated using the Mutate module in VMD [53]. The free energy profiles of ion permeation were computed as described in the Supplementary material.

2.2. Brownian dynamics simulations

All BD inputs were created with the GCMC/BD module [47] of the CHARMM GUI server [54] and all simulations were performed using the GCMC/BD program [55] (for further simulation details see SI). The equilibrium BD simulation time of the mVDAC1 crystal structure was 0.5, 0.4, 0.2, 0.15, 0.1, 0.05, 0.05 and 0.05 μs at 0.1 , 0.2 , 0.4 , 0.6 , 0.8 , 1.0 , 1.2 , and 1.4 M KCl, respectively. These simulations were used to evaluate the distribution of ions in the pore. The conductance of the mVDAC1 crystal structure, the hVDAC1 mixed crystal/NMR structure (PDB ID: 2JK4 [33]), and the hVDAC1 NMR conformation #3 (NMR3; (PDB ID: 2K4T [32]) was determined in the absence of a salt gradient from 0.5 μs BD trajectories in 0.1 M KCl and NaCl concentration at ±50 mV and from 0.05 μs BD trajectories in 1.0 M KCl concentration at ±100 mV. The reversal potential and the conductance were also computed from non-equilibrium 0.2 μs BD simulations performed in 1.0 M/0.1 M (*trans*/*cis*) KCl and NaCl gradients respectively, applying a membrane potential ranging from −50 mV to 50 mV with a stepsize of 10 mV. To get satisfactory statistical convergence all BD simulations were repeated 10 times each using a different set of random numbers. Each point calculation took about 14 h using a single cpu (Quad-Core 2.3 GHz AMD Opteron Processor). The free energy profiles of ion permeation were computed as described in the Supplementary material.

3. Results

In the first part of this study (see Sections 3.1 and 3.2), we examined the molecular basis for the selectivity and conductance of VDAC1 wt using BD simulations performed on the mammalian structures.

The ion distributions at different salt concentrations computed by BD on mVDAC1 structure were compared to previously published data obtained from equilibrium MD [29] and confronted to experimental measurements. Because of the deviation observed for mVDAC1 between the computed and the experimental selectivity, we investigated, in the second part of the study (see Section 3.3), the impact of the protein flexibility on the selectivity and conductance computed from BD simulations performed on different MD conformations. The third part (see Sections 3.4 and 3.5) of this work is devoted to the study of the ion transport through several mVDAC1 single point mutant proteins using MD and BD approaches in order to gain a more detailed insight into the molecular mechanism determining VDAC selectivity.

3.1. Ion distribution in mVDAC1 wt at different KCl concentrations

The distribution of ions inside the pore was estimated from equilibrium BD simulations performed on the mVDAC1 crystal structure at different KCl concentrations ranging from 0.1 M to 1.4 M. The computed time-averaged number of chloride (N_{Cl}-) and of potassium ions ($N_K{}^+$) inside the pore, as well as the N_{Cl}-/$N_K{}^+$ ratio, a measure of VDAC preference towards anions, clearly vary with the bulk ionic concentration (Fig. 1 and Fig. 5): N_{Cl}- and $N_K{}^+$ increase with increasing KCl concentration whereas the N_{Cl}-/$N_K{}^+$ ratio decreases. The dependence of the N_{Cl}-/$N_K{}^+$ ratio with salt concentration is in remarkable agreement with that obtained from MD trajectories [29] (Fig. 1) albeit the N_{Cl}- and $N_K{}^+$ numbers derived from all BD simulations are lower than their corresponding MD values (see Supplementary material for more details). Both approaches thus describe a congruent concentration-dependent preference of VDAC for anions.

3.2. Conductance and selectivity of VDAC1 wt

3.2.1. Selectivity of VDAC1 wt

The reversal potential is the electric potential difference at zero net current and is determined from I/V curves. These curves were calculated from BD simulations performed on mVDAC1 structure in a tenfold 1.0 M/0.1 M KCl concentration gradient in the presence of a transmembrane electrical potential difference (Fig. S2). The reversal potential is a measure of the selectivity of the channel: a positive value indicates a preference towards anions. On mVDAC1 the computed reversal potential value is 16.6 mV indicating indeed an anionic selective channel. It is about 5 mV higher than the experimental values (about 10–12 mV) measured on VDAC proteins from fungi, insects, mammals and plants [16–22,56] (Table 1). One can provide different reasons to explain this discrepancy. First one cannot exclude that the crystal and physiological structures of mVDAC1 show differences that would affect the selectivity. Second the BD method suffers from a number of approximations that may impact the computed value of selectivity. For instance a recent paper [47] showed that a decrease of about 10 to 20% in the selectivity can be observed using different scaling methods for the diffusion coefficient of the ions inside the pore. Third the computed value was determined on a single conformation that represents the average structure in the crystal whereas the experimental data are average values obtained from several individual measurements.

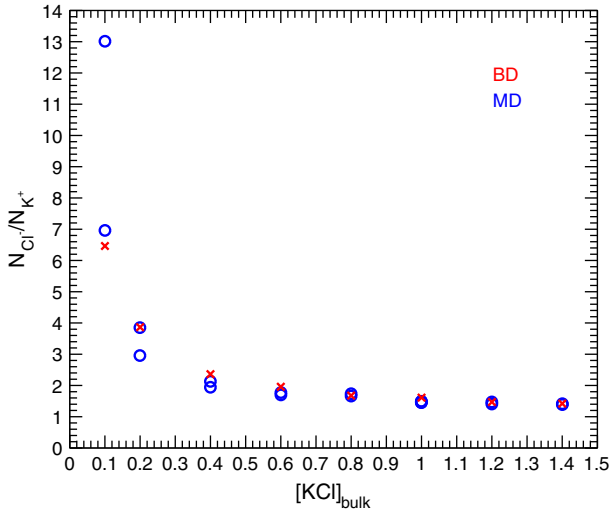

Fig. 1. Ion distribution inside mVDAC1. Concentration dependence of the N_{Cl}-/$N_K{}^+$ ratio with the bulk ionic concentration computed from MD (circle) and BD (cross) simulations.

Our computed reversal potential value for mVDAC1 is slightly higher than the value calculated on the same structure using a Poisson–Nernst–Planck (PNP) equation [48] suggesting that the approximations made in the BD approach relative to those in PNP may contribute to the discrepancy between the computed and experimental selectivity (see Supplementary material for details). However another or concomitant possible explanation is that irrespective of the experimental conditions used measures performed in separate experiments were reported to differ from each other by up to 10 mV [24]. In that respect our value can be regarded as in satisfactory agreement with the experimental data.

The inversion of the concentration gradient (0.1 M/1.0 M KCl *cis*/*trans*) does not significantly affect the computed value of the reversal potential (Table 1), indicating a symmetrical ion free energy barrier. This last result contrasts with the one obtained from BD simulations of the mixed NMR/Xray hVDAC1 structure [47] but is in agreement with a PNP calculation on mVDAC1 [48].

A quite large dispersion in the reversal potential was also obtained from BD calculations on the 20 NMR conformations of hVDAC1 performed in a 1.0 M/0.1 M KCl gradient [45]. A few of these conformations featured a very good agreement of its reversal potential with the experimental average value, in particular the conformer 3 (NMR3) with $\Delta V_{rev} \approx 1$ mV. Likewise a BD study performed on the mixed NMR/crystal structure of hVDAC1 gave rise to a computed reversal potential [47] also close to the experimental data ($\Delta V_{rev} \approx 2$ mV) [47]. All these results prompted us to calculate the reversal potential from BD simulations on the mixed crystal/NMR structure and on the NMR3 conformer of hVDAC1. The values are almost identical to those previously published (Table S1, [45,47]) ruling out that differences in the simulation parameters could explain our higher reversal potential computed for mVDAC1.

We also performed BD simulations of mVDAC1 and of the K20S mVDAC1 mutant in a 1.0 M/0.1 M NaCl gradient. A chloride selectivity higher in NaCl than in KCl is obtained for the wt (Table 1). Furthermore the anion selectivity computed for the K20S mutant is significantly decreased relative to that of the wt. These two results are in agreement with measurements made on *N. crassa*, rat, and mouse VDAC [57].

Comparison of our BD values with experimental data indicates that the BD approach despite its approximations, a fixed protein structure and a continuum description of the solvent, can simulate fairly well several aspects of VDAC selectivity. Our calculations on the different experimental structures therefore suggest that the deviation of the selectivity value computed on mVDAC1 from the experimental data may lie in part in some particular features of the mouse crystal structure.

3.2.2. Conductance of VDAC1 wt

The conductance of mVDAC1 was computed from BD simulations performed in various symmetric conditions of KCl (0.1 M and 1.0 M) and of NaCl (1.0 M) (see Table 1). In 1.0 M KCl solution, the conductance is about 1 nS lower than the average experimental values (about 4 nS) measured on the open state of VDAC from different species [10,12,22,58]. A closer look at the experimental distribution of

Table 1
Electrophysiological properties of mVDAC1. Reversal potential determined from non-equilibrium BD simulations and channel conductance determined from equilibrium BD simulations of the mVDAC1 wt and K20S mutant in potassium and sodium chloride.

Salt	Protein	Reversal potential in 1.0 M/0.1 M (0.1 M/1.0 M) [mV]		Conductance in 1.0 M [nS]			Conductance in 0.1 M [nS]		
		BD	Exp.	BD		Exp.	BD		Exp.
				−100 mV	100 mV		−50 mV	50 mV	
KCl	wt	16.6 ± 2.4 (−17.8 ± 2.3)	10.2–11.8[a]	2.9 ± 0.3	2.6 ± 0.4	3.7–4[b]	0.5 ± 0.1	0.5 ± 0.1	0.45–0.58[c]
NaCl	wt	23.4 ± 2.1	17–21[d]	2.8 ± 0.5	2.7 ± 0.3	3–4[e]	–	–	
	K20S	11.7 ± 2.2	6[d]	2.4 ± 0.5	2.6 ± 0.5	3.3[f]	–	–	

[a] *Heliothis virescens*, mais VDAC, mVDAC1 and yVDAC1[16–22,56].
[b] *N. crassa* VDAC, mVDAC1 [31,64].
[c] yVDAC, rat, maize, and bean VDAC [16,19,23,30].
[d] Rat, mouse and *N.crassa* VDAC [57].
[e] *N.crassa*, *Dictostelium discoidem*, rat VDAC, mVDAC1 and yVDAC [23,58–62].
[f] mVDAC1[57].

conductance measures shows that the variation around the average value of the measured conductances is at least 0.5 nS (see Fig. 2 in [10]; Fig. 3 in [58]). Our values hence are not comprised within the range of these values and slightly underestimate the experimental measured conductance at 1.0 M KCl. Unlike the reversal potential the exchange of KCl by NaCl only slightly affects the conductance (Table 1). Different values (ranging from 3 to 4 nS) have been measured for VDAC conductance in 1.0 M NaCl [23,58–62] suggesting, like the BD calculations, that the conductance of VDAC might not differ significantly between 1.0 M NaCl and KCl.

At 0.1 M KCl solution the computed conductance is about 0.5 nS in excellent agreement with the average experimental data measured on fungi, mammalian and plant VDAC which range from 0.44 to 0.58 nS depending on the species [11,23,58] (Table 1).

A possible explanation for the discrepancy at 1.0 M salt could arise from the use in BD of a pre-calculated electrostatic potential assuming a bulk salt concentration throughout the pore that could reduce the computed conductance at 1.0 M in a more notable way than at 0.1 M.

For the sake of comparison we also computed the conductance on the mixed crystal/NMR structure and NMR3 of hVDAC1 (see Table S1). Our values are close to those calculated in other BD studies performed on the same structures [45,47]. In contrast to the reversal potential the conductance value barely depends on the 3D structure with the exception of the mixed NMR/Xray hVDAC1 at 0.1 M KCl (Table S1 to be compared with Table 1).

3.3. Influence of the local conformation on the BD electrophysiological properties

In Section 3.2.1 our results suggested that the crystal structure of mVDAC1 present features accountable for its higher computed reversal potential relative to that of the hVDAC1 structures (Table 1, Table S1, [45,47,48]). To explore the relevance of this conjecture we investigated the impact of local fluctuations of the 3D structure on the calculated selectivity by performing BD simulations of 10 conformations (named conf1–10) extracted from a 150 ns MD simulation of mVDAC1 wt (see Supplementary material; Tables S2 and S3, and Fig. S3).

3.3.1. The selectivity and the conductance of mVDAC1 MD conformations

The reversal potential and conductance values were determined from the BD trajectories carried out on the 10 MD wt conformations in an asymmetric 1.0 M/0.1 M KCl solution for several values of the transmembrane potential. As shown in Fig. 2A, the 10 protein conformations feature different reversal potential and conductance values. The largest difference among the conformations is about 17 mV for the reversal potential and 0.8 nS for the conductance. The reversal potential value closest to the average experimental data is 14.2 mV (obtained for conf4; Table S4). Several conformations feature a conductance close to the average experimental value of 1.8 nS at 1.0 M/0.1 M KCl for yVDAC1 [17] (conf1-3 and 6; Table S4). No correlation is found however between the channel conductance and the reversal potential values as a function of the conformation number. In support of this observation electrophysiological measurements have shown that a conductance state may be characterized bya broad range of reversal potential values (including a sign inversion) [24,63].

3.3.2. The BD equilibrium energy profile for ion permeation through mVDAC1

To further explore the importance of conformational fluctuations on the selectivity and conductance multi-ion free energy profiles of chloride and potassium permeation were computed using the BD simulations carried out in a symmetric 0.2 M KCl solution on three different conformations of mVDAC1: the crystal structure and two selected MD snapshots (conf4 and 8) (Fig. 2B). The two MD conformations were chosen as their reversal potential ranges from the closest (conf4) to the most distant (conf8) value to the experimental one [16–22,56]. The chloride and potassium permeation energy profiles through the crystal structure are very similar to the ones described in an earlier MD study [29]. Significant changes in these profiles are observed for conf4 and conf8 (for more details see Supplementary material). The comparison of the free energy profiles suggests that the difference in selectivity computed for these conformations may arise from differences localized at about the middle of the pore where the N-terminal helix is located. On the structural level the positive charge of several residues (Supplementary material; Table S5 and Fig. S4) is less shielded in conf8 which could explain the altered energy profiles and as a consequence the high reversal potential of this conformation.

3.4. MD study of mVDAC1 mutants

Single charged residues were shown, in site-directed mutagenesis experiments, to affect the selectivity of yVDAC1 [17,18,25]. PNP calculations carried on a few mVDAC1 mutants and BD simulations performed on hVDAC1 variants (NMR3) corroborated these experimental data [45,48]. PNP and BD approaches ignore the flexibility of the protein and the detailed hydration of the charged species and thus might fail to determine the molecular reasons for the changes in the selectivity upon the substitution of a single charged residue. In that respect MD approach could be a more adequate method as it includes protein structural dynamics and hydration.

We thus investigated by MD the transport of ions through five mutants whose selectivity in yVDAC1 was reported to be affected in different ways and that are conserved between yeast and mammals. Experiments clearly show that the introduction of several point

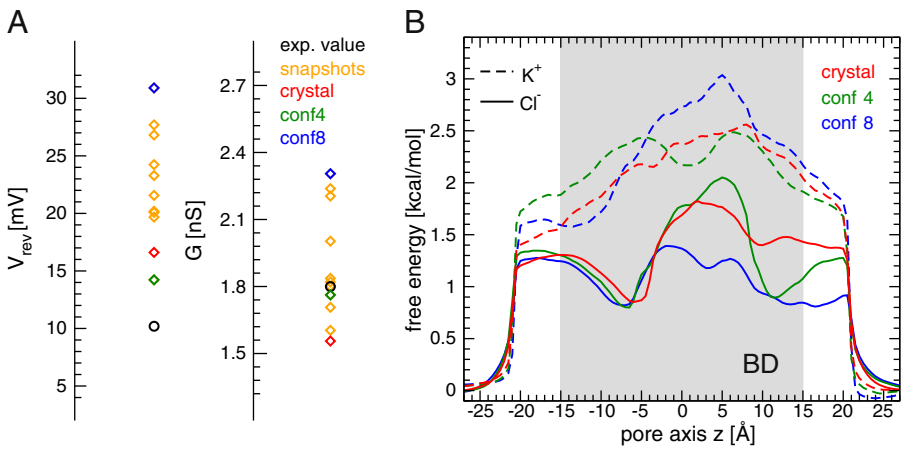

Fig. 2. BD electrophysiological properties of different mVDAC1 conformations. (A) Reversal potential and conductance values of the wt crystal structure (red diamonds) and conformations extracted from MD trajectories (orange diamonds) computed from BD simulations at 1.0 M/0.1 M KCl. The experimental value (black circle) is also depicted. Conformations discussed in the text are highlighted as green and blue diamonds (conf4 and conf8, respectively). (B) Free energy profile for Cl^- (solid line) and K^+ (dashed line) permeation computed from the BD simulations of the crystal structure (red), conf4 (green), and conf8 (blue). An error calculation is shown in Fig. S13 for the wt crystal structure. The region corresponding to the pore is highlighted in gray.

mutations in yVDAC1 do not influence the conductance of the channel suggesting that no conformational change prone to induce a decrease in conductance occurs upon mutation [17,18,25]. This finding endorses the use of a modeled *in-silico* mutant structure for further investigation. We therefore performed detailed all-atom equilibrium 150 ns MD simulations of the mVDAC1 wt and point mutants, namely K20E, D30K, K61E, E158K and K252E (numbering refers to mammalian sequences), in a 0.2 M KCl solution (see Section 2.1 and Supplementary material).

3.4.1. The anion preference of mVDAC1 is sensitive to specific charged residue substitutions

The N_{Cl}-/$N_K$$^+$ ratio inside the pore computed using the equilibrium MD trajectories was used to describe the ion preference of VDAC wt and mutants. As shown in Fig. 3B, this ratio is comparable for the wt, K252E and E158K mutant proteins indicating a similar preference towards anions. The D30K mutant channel reveals a preference for anions higher than the wt whereas the K20E and K61E mutants feature a lower preference for anions (Table S6). A strong decrease in anion selectivity is observed for K20E but not a reversed selectivity as experimentally measured in yVDAC1. Overall, the agreement between the computed and experimental selectivity values is fairly good.

3.4.2. Specific interactions, pathways and electrostatic properties in the MD trajectories

We analyzed the wt and mutant protein trajectories to search for specific ion–protein interactions and/or specific ion pathways through the pore. No specific long-lived (≥5 ns) interactions as well as no pathways were identified except in the E158K mutant trajectory which features a single long-lived salt bridge (see Fig. S5–S8) formed far from the location of the K158 and hence unlikely to ensue from the mutation itself (see SI).

Local changes in the electrostatic potential are observed in the vicinity of the mutated residues (Fig. S9). Moreover the electric field arising from the protein averaged over each MD trajectory indicates the occurrence of an electrostatic force attracting anions from both sides of the pore in all proteins. Differences in the electric field of the different variants are seen, in particular around the N-terminal helix region (Fig. S10): the electric field is stronger in the more anion-selective D30K mutant whereas it is weaker in the moderately anion selective K61E mutants relative to that arising in the wt proteins. These data together with the absence of specific ion pathways and long-lasting ion–protein interactions support the idea that changes in VDAC selectivity due to point charged residue substitution originate from variations in the electrostatic properties arising from the distribution of fixed charges in the pore, notably in the vicinity of the N-terminal helix.

3.4.3. The energy landscape of ion permeation in mutants featuring a change in selectivity is altered

The multi-ion free energy profiles of chloride and potassium permeation were computed along the pore axis (Fig. 4) from the wt and the five mutant trajectories. The free energy profile of the wt at 0.2 M KCl (Fig. 4A) is similar to the previously published profile for mVDAC1 at 0.1 M KCl [29].

The energy profile of chloride permeation computed for E158K and K252E mutants resemble the wt profile though the barrier separating the two wells is slightly flattened. The K^+ profile also looks comparable with however a first higher maximum and the quasi absence of the minimum well in K252E. These changes may explain the slightly enhanced (about 10%) N_{Cl}-/$N_K$$^+$ ratio for E158K and K252E mutant relative to the wt (Fig. 4A, Table S6).

In contrast, the permeation profiles of the K20E, D30K and K61E mutants are significantly altered relative to the wt (see Fig. 4B, C). In the case of the K20E and K61E mutants the depth of the first energy well in the Cl^- profile is drastically reduced and the first energy barrier for potassium is significantly lowered facilitating the crossing of K^+. These results agree with less anion-selective channels. The permeation profile of the K61E mutant shows a first energy minimum for potassium lower than the minimum for chloride, explaining thereby the low N_{Cl}-/$N_K$$^+$ ratio of this mutant protein compared to that of the K20E mutant.

For the D30K mutant, only one large caldera-like minimum occurs in the Cl^- profile and the two energy barriers separated by an energy well in the wt are replaced by one single higher barrier in the K^+ profile. This generates an energy difference between Cl^- and K^+ permeation larger than in the wt in agreement with the higher anion selectivity measured for the D30K mutant.

The major changes in the energy profile between the mutants with an altered selectivity and the wt take place in a region of the barrel located around the N-terminal helix. This region appears to be particularly important for VDAC selectivity.

3.5. BD study of mVDAC1 mutants

Our detailed all-atom MD simulations on mVDAC1 wt and mutant proteins clearly showed that the effect of substitution of residues

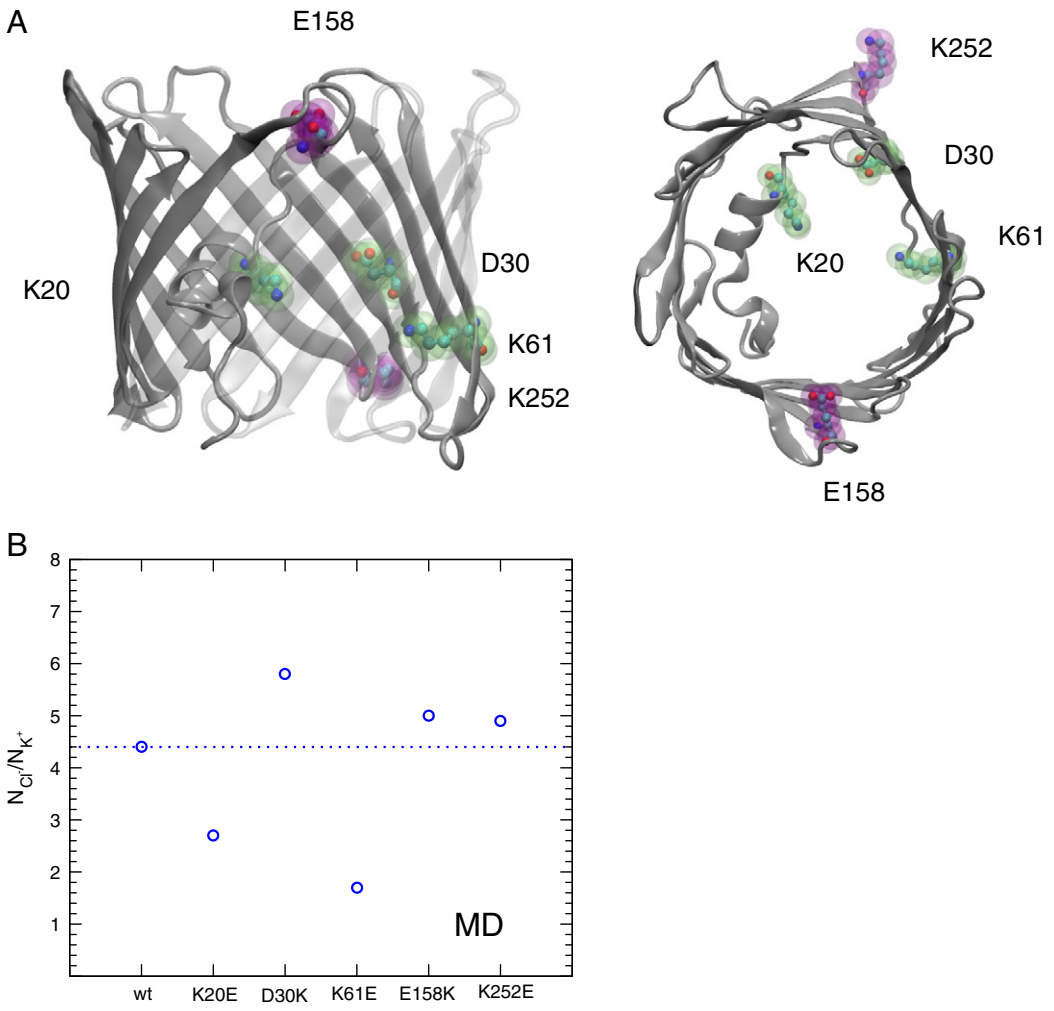

Fig. 3. MD N_{Cl^-}/N_{K^+} ratio of different mVDAC1 mutants. (A) Two views rotated by 90° of the localization in the mVDAC1 3D structure of the selected K20, D30, K61, E158 and K252 residues. The protein is depicted as a gray cartoon. The charged residues to be mutated are highlighted as van-der-Waals spheres colored in green and magenta according to their impact on the selectivity (see text). The image was prepared using vmd [53] using the crystal structure (PDB ID: 3EMN [31]). (B) The N_{Cl^-}/N_{K^+} ratio for the wt, K20E, D30K, K61E, E158K and K252E mutants computed from 150 ns MD trajectories in 0.2 M KCl.

located in the pore can be attributed to a change in the electrostatic properties of the pore, with a major contribution from the region localized roughly halfway of the channel, and not to the formation of long-lived ion–protein interactions or to specific translocation pathways. The level of detail in all-atom MD trajectories which are quite computationally demanding and require long simulation times to sample enough ion transport events may thus be not needed to study the electrophysiological properties (selectivity, conductance) of VDAC. As the electrostatics of VDAC plays a major role in ion flow BD approach appears as a pertinent and less computationally expensive method as shown in this study and in others [45,47,50].

BD simulations of several mVDAC1 variants were first performed in asymmetric (1.0 M/0.1 M) KCl solution to compare the conductance and the reversal potential values of the five mutant proteins to the wt data. Equilibrium BD simulations of these mutants were also carried out in symmetrical conditions (0.2 M KCl) to compare the ion permeation energy profiles to the MD ones. To palliate the absence of protein flexibility in the BD approach several structures of the mutant protein were modeled based either on the crystal structure or on 10 protein conformations extracted from the MD trajectories.

3.5.1. Reversal potential and conductance of mutant mVDAC1 proteins

As previously observed for the wt (see Section 3.3.2) the conductance and reversal potential values differ for all 11 conformations of the five mutants (Fig. S11, Table S7). The variability of the reversal potential of the different conformations ranges between about 6 mV (for D30K) and 20 mV (for K20E). The computed conductance values also show a certain variability upon the conformation (about 0.5 nS for K20E and 1 nS for D30K).

For the sake of clarity, we will next focus on the data obtained for the crystal structure and for the MD conformation having the computed reversal potential value closest to the experimental data (Fig. 5). The data for the other conformations can be found in Table S7. The reversal potential values of the two K252E and E158K mutant conformations are close to that of the wt, whereas the reversal potential of the K20E, D30K and K61E mutants are significantly altered [17,18]. The K20E and the K61E mutants modeled using the mVDAC1 crystal structure as a template give a reversed selectivity (indicated by a negative reversal potential) lower than the average experimental value. The same mutants modeled from the MD snapshot produce a reversal potential closer to the experimental value and no inversion of the selectivity. The D30K mutant built either from the crystal structure or from the MD snapshot features a selectivity higher than the wt, the E158K or the K252E mutant in accord with experimental data [17,18] albeit the effect of this mutation is overestimated. Overall the variation in the computed reversal potential among the wt and mutant proteins follows the same trend as experimentally observed (Fig. 5).

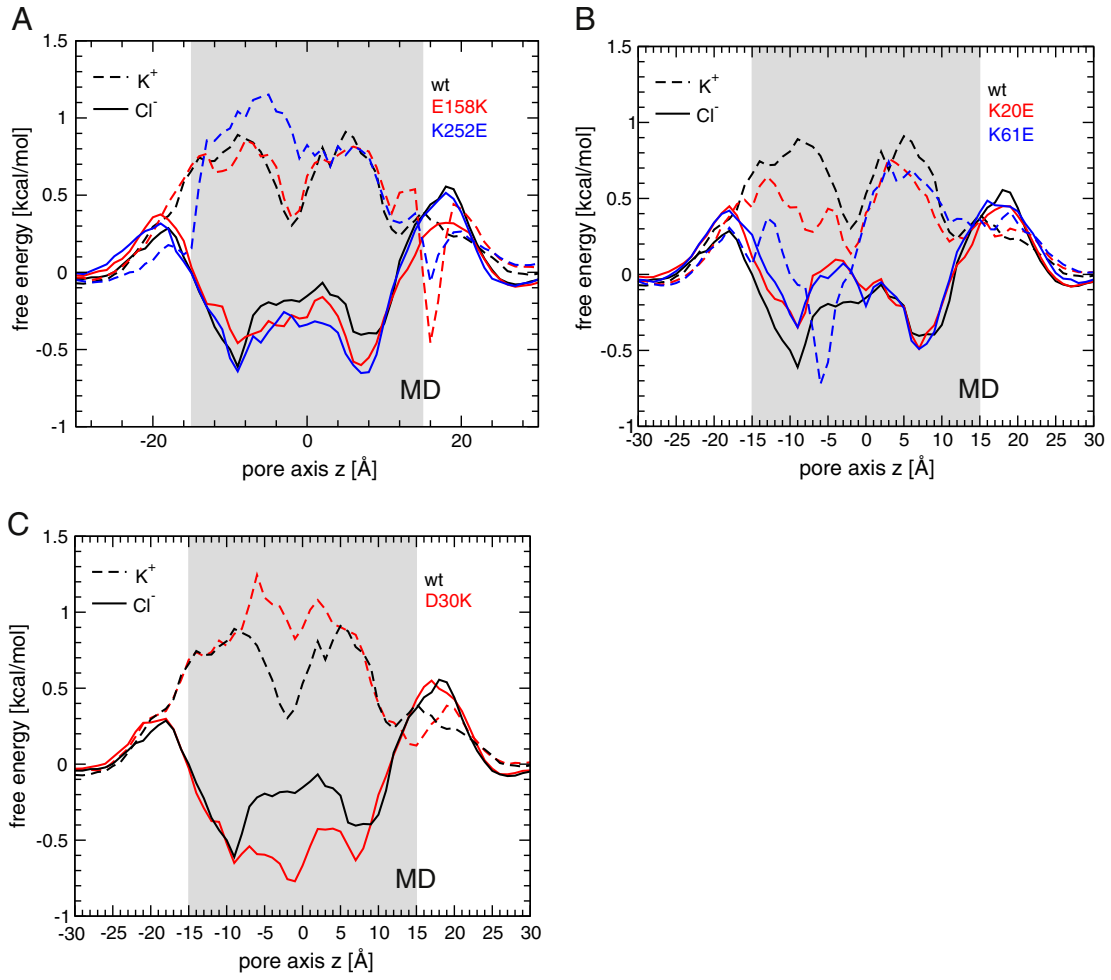

Fig. 4. MD ion permeation free energy profiles for mVDAC1 mutants (A) The energy profile of potassium (dashed line) and chloride (solid line) permeation through mVDAC1 wt (black), the E158K (red) and the K252E (blue) mutant. (B) The energy profile of potassium (dashed line) and chloride (solid line) permeation through mVDAC1 wt (black), the K20E (red) and the K61E (blue) mutant. (C) The energy profile of potassium (dashed line) and chloride (solid line) permeation through mVDAC1 wt (black) and the D30K (red). An error calculation is shown in Fig. S13 for the wt crystal structure. The region corresponding to the pore is highlighted in gray.

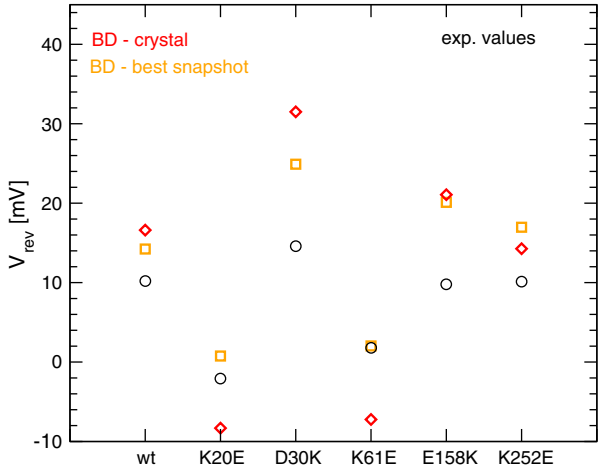

Fig. 5. Comparison between the experimental and computed reversal potential of mVDAC1 mutants and of the wt. The experimental values taken from [17] and the calculated BD values based on the crystal structure are shown as circles and diamonds respectively. In addition the conformation with the closest BD value of the reversal potential to the experimental data is shown as squares. A complete list of calculated BD values is given in Table S4 and S7.

3.5.2. Free energy profile, specific interactions and pathways

The free energy profiles of chloride and potassium permeation computed from BD trajectories are in a relative good agreement with the MD profiles (Fig. S12). Moreover, BD trajectories like the MD simulations show no specific protein–ion interactions as well as no particular ion pathways. The good agreement between MD and BD results furthermore endorses the use of BD for the study of the electrophysiological properties of VDAC mutants. Since the influence of the protein on ion diffusion is mainly of electrostatic nature in BD, these results once more stress the importance of the electrostatic features of VDAC pore with respect to its selectivity.

4. Discussion

Quite extensive BD simulations of mVDAC1 wt and mutants in conjunction with MD simulations were performed to elucidate the factors governing ion flow through VDAC. Noticeably the electrophysiological properties computed on the mVDAC1 recombinant structure by BD and MD are in fairly good agreement with the experimental data measured on native proteins.

The distribution of ions inside the pore computed from BD simulations across mVDAC1 structure at different salt concentrations indicates an anionic preference as experimentally reported. Furthermore the ion distribution ratio decreases with increasing salt concentration in agreement with experimental data obtained on VDAC from

different species [18,25,29] and with a recent MD study [29]. This loss of selectivity at high concentration reflects the screening of the permanent charges of the protein by counter-ions. The ability of BD to depict the distribution of ions in agreement with MD and experimental data may be promoted by the relative rigidity of the structure of the barrel and the weak dehydration of permeating ions.

The computed selectivity and conductance values portrayed the three VDAC1 high resolution structures as anionic channels in agreement with experiments. Notwithstanding, the value of the reversal potential computed for the mVDAC1 crystal structure deviates more from the experimental data than that computed using the hVDAC1 structures. The BD simulations performed on several protein conformations randomly extracted from a MD simulation of the mVDAC1 wt indicate that the computed reversal potential is rather sensitive to the local protein conformation, in particular to the solvent-accessibility of charged residues in the pore and to the formation/rupture of ionic interactions between charged residues.

Voltage-dependence studies of VDAC have shown that one conductance state, for instance the open state, can feature different (even reverse) selectivity values [24,30,63]. This could be explained by the existence of several "selectivity states" that would differ from each other by modest structural changes which would not affect the conductance. The molecular origin of these structural changes is beyond the scope of this work. However the comparison of the experimental 3D structures may give some hints. The mVDAC1 crystal structure and the hVDAC1 mixed NMR/Xray structures which are both regarded as depicting the open state, are remarkably similar apart from the orientation of the N-terminal helix, which is turned by almost 90° between the two structures. In the mVDAC1 structure the charged residues of the N-terminal helix are almost completely solvent exposed and oriented towards the pore unlike those in the hVDAC1 structure. These differences could result in different selectivity values as indeed shown in our BD calculations.

To further investigate the molecular origin of the selectivity of the pore, we studied using MD and BD simulations the ion transport of mVDAC1 mutants some of which feature an altered selectivity relative to VDAC wt [17]: K20E (cation-selective), K61E (less anion-selective), D30K (more anion-selective), E158K and K252E (wt-like). The ion preference computed from MD equilibrium simulations and the selectivity computed from BD simulations of wt and mutant proteins are in good agreement with experimental data. A strong reduction/inversion of the selectivity in K20E, a reduction in selectivity in K61E, an increased selectivity in D30K and a wt-like selectivity in E158K and K252K are observed. Equilibrium MD and BD simulations led to similar ion permeation profiles of either wt or mutants. These profiles show alterations due to mutations of charged residues in agreement with the measured changes in selectivity. They furthermore indicate that the region of the pore encompassing a girdle of the barrel around the N-terminal helix appears as a key player in the control of the channel selectivity.

The overall 0.9 μs MD and 12 μs BD trajectories on VDAC1 wt and mutants suggest that the change in selectivity of the K20E, D30K and K61E proteins ensues not from the existence of distinct ion pathways and/or the formation specific long-lived ion–protein interactions but from a change in the electric field inside the pore arising from the alteration of the charge distribution. Thus, altogether our study clearly shows that the selectivity is mainly determined by the electrostatic pattern of the pore. If this pattern is altered by specific site mutations or by changes in the protein structure or else is screened by a high ionic concentration then the selectivity is altered accordingly.

Supplementary data to this article can be found online at http://dx.doi.org/10.1016/j.bbamem.2012.12.018.

Acknowledgements

EMK thanks the IRISIB (Brussels region) for the BB2B fellowship. This work was also supported by the ARC grant number 20052 (Communauté française de Belgique). FH is a Research Director and MP is a Senior Research Associate at the FRS-FNRS (Belgium).

References

[1] M. Colombini, Structure and mode of action of a voltage dependent anion-selective channel (VDAC) located in the outer mitochondrial membrane, Ann. N. Y. Acad. Sci. 341 (1980) 552–563.
[2] E. Rapizzi, P. Pinton, G. Szabadkai, M.R. Wieckowski, G. Vandecasteele, G. Baird, R.A. Tuft, K.E. Fogarty, R. Rizzuto, Recombinant expression of the voltage-dependent anion channel enhances the transfer of Ca2+ microdomains to mitochondria, J. Cell Biol. 159 (2002) 613–624.
[3] K.S. McCommis, C.P. Baines, The role of VDAC in cell death: friend or foe? Biochim. Biophys. Acta 1818 (2012) 1444–1450.
[4] V. Shoshan-Barmatz, P. De, V.M. Zweckstetter, Z. Raviv, N. Keinan, N. Arbel, VDAC, a multi-functional mitochondrial protein regulating cell life and death, Mol. Aspects Med. 31 (2010) 227–285.
[5] E. Bustamante, H.P. Morris, P.L. Pedersen, Energy metabolism of tumor cells. Requirement for a form of hexokinase with a propensity for mitochondrial binding, J. Biol. Chem. 256 (1981) 8699–8704.
[6] J.G. Pastorino, N. Shulga, J.B. Hoek, Mitochondrial binding of hexokinase II inhibits Bax-induced cytochrome c release and apoptosis, J. Biol. Chem. 277 (2002) 7610–7618.
[7] N. Majewski, V. Nogueira, P. Bhaskar, P.E. Coy, J.E. Skeen, K. Gottlob, N.S. Chandel, C.B. Thompson, R.B. Robey, N. Hay, Hexokinase–mitochondria interaction mediated by Akt is required to inhibit apoptosis in the presence or absence of Bax and Bak, Mol. Cell 16 (2004) 819–830.
[8] F. Homblé, E.M. Krammer, M. Prévost, Plant VDAC: facts and speculations, Biochim. Biophys. Acta 1818 (2012) 1486–1501.
[9] A. Messina, S. Reina, F. Guarino, V. De Pinto, VDAC isoforms in mammals, Biochim. Biophys. Acta 1818 (2012) 1466–1476.
[10] R. Benz, Permeation of hydrophilic solutes through mitochondrial outer membranes: review on mitochondrial porins, Biochim. Biophys. Acta 1197 (1994) 167–196.
[11] M. Colombini, Voltage gating in the mitochondrial channel, VDAC, J. Membr. Biol. 111 (1989) 103–111.
[12] H. Abrecht, R. Wattiez, J.M. Ruysschaert, F. Homblé, Purification and characterization of two voltage-dependent anion channel isoforms from plant seeds, Plant Physiol. 124 (2000) 1181–1190.
[13] M. Colombini, VDAC: the channel at the interface between mitochondria and the cytosol, Mol. Cell. Biochem. 256–257 (2004) 107–115.
[14] T. Hodge, M. Colombini, Regulation of metabolite flux through voltage-gating of VDAC channels, J. Membr. Biol. 157 (1997) 271–279.
[15] X. Xu, W. Decker, M.J. Sampson, W.J. Craigen, M. Colombini, Mouse VDAC isoforms expressed in yeast: channel properties and their roles in mitochondrial outer membrane permeability, J. Membr. Biol. 170 (1999) 89–102.
[16] D.M. Adelsberger-Mangan, M. Colombini, Elimination and restoration of voltage dependence in the mitochondrial channel, VDAC, by graded modification with succinic anhydride, J. Membr. Biol. 98 (1987) 157–168.
[17] E. Blachly-Dyson, S. Peng, M. Colombini, M. Forte, Selectivity changes in site-directed mutants of the VDAC ion channel: structural implications, Science 247 (1990) 1233–1236.
[18] S. Peng, E. Blachly-Dyson, M. Forte, M. Colombini, Large scale rearrangement of protein domains is associated with voltage gating of the VDAC channel, Biophys. J. 62 (1992) 123–131.
[19] D.P. Smack, M. Colombini, Voltage-dependent channels found in the membrane fraction of corn mitochondria, Plant Physiol. 79 (1985) 1094–1097.
[20] M. Forte, D. Adelsberger-Mangan, M. Colombini, Purification and characterization of the voltage-dependent anion channel from the outer mitochondrial membrane of yeast, J. Membr. Biol. 99 (1987) 65–72.
[21] C. Doring, M. Colombini, Voltage dependence and ion selectivity of the mitochondrial channel, VDAC, are modified by succinic anhydride, J. Membr. Biol. 83 (1985) 81–86.
[22] M. Colombini, Purification of VDAC (voltage-dependent anion-selective channel) from rat liver mitochondria, J. Membr. Biol. 74 (1983) 115–121.
[23] N. Roos, R. Benz, D. Brdiczka, Identification and characterization of the pore-forming protein in the outer membrane of rat liver mitochondria, Biochim. Biophys. Acta 686 (1982) 204–214.
[24] D.W. Zhang, M. Colombini, Group IIIA-metal hydroxides indirectly neutralize the voltage sensor of the voltage-dependent mitochondrial channel, VDAC, by interacting with a dynamic binding site, Biochim. Biophys. Acta 1025 (1990) 127–134.
[25] E.B. Zambrowicz, M. Colombini, Zero-current potentials in a large membrane channel: a simple theory accounts for complex behavior, Biophys. J. 65 (1993) 1093–1100.
[26] M.J. Holden, M. Colombini, The mitochondrial outer membrane channel, VDAC, is modulated by a soluble protein, FEBS Lett. 241 (1988) 105–109.
[27] U.R. Wunder, M. Colombini, Patch clamping VDAC in liposomes containing whole mitochondrial membranes, J. Membr. Biol. 123 (1991) 83–91.
[28] M. Colombini, Pore size and properties of channels from mitochondria isolated from *Neurospora crassa*, J. Membr. Biol. 53 (1980) 79–84.
[29] E.M. Krammer, F. Homblé, M. Prévost, Concentration dependent ion selectivity in VDAC: a molecular dynamics simulation study, PLoS One 6 (2011) e27994.
[30] L. Mlayeh, S. Chatkaew, M. Leonetti, F. Homblé, Modulation of plant mitochondrial VDAC by phytosterols, Biophys. J. 99 (2010) 2097–2106.
[31] R. Ujwal, D. Cascio, J.P. Colletier, S. Faham, J. Zhang, L. Toro, P. Ping, J. Abramson, The crystal structure of mouse VDAC1 at 2.3 A resolution reveals mechanistic insights into metabolite gating, Proc. Natl. Acad. Sci. U. S. A. 105 (2008) 17742–17747.

[32] S. Hiller, R.G. Garces, T.J. Malia, V.Y. Orekhov, M. Colombini, G. Wagner, Solution structure of the integral human membrane protein VDAC-1 in detergent micelles, Science 321 (2008) 1206–1210.
[33] M. Bayrhuber, T. Meins, M. Habeck, S. Becker, K. Giller, S. Villinger, C. Vonrhein, C. Griesinger, M. Zweckstetter, K. Zeth, Structure of the human voltage-dependent anion channel, Proc. Natl. Acad. Sci. U. S. A. 105 (2008) 15370–15375.
[34] V. De Pinto, G. Prezioso, F. Thinnes, T.A. Link, F. Palmieri, Peptide-specific antibodies and proteases as probes of the transmembrane topology of the bovine heart mitochondrial porin, Biochemistry 30 (1991) 10191–10200.
[35] M. Colombini, The published 3D structure of the VDAC channel: native or not? Trends Biochem. Sci. 34 (2009) 382–389.
[36] F. Al Bitar, N. Roosens, M. Smeyers, M. Vauterin, J. van Boxtel, M. Jacobs, F. Homblé, Sequence analysis, transcriptional and posttranscriptional regulation of the rice vdac family, Biochim. Biophys. Acta 1625 (2003) 43–51.
[37] M. Colombini, VDAC structure, selectivity, and dynamics, Biochim. Biophys. Acta 1818 (2012) 1457–1465.
[38] M.J. Young, D.C. Bay, G. Hausner, D.A. Court, The evolutionary history of mitochondrial porins, BMC Evol. Biol. 7 (2007) 31.
[39] H. Abrecht, E. Goormaghtigh, J.M. Ruysschaert, F. Homblé, Structure and orientation of two voltage-dependent anion-selective channel isoforms. An attenuated total reflection fourier-transform infrared spectroscopy study, J. Biol. Chem. 275 (2000) 40992–40999.
[40] X.W. Guo, P.R. Smith, B. Cognon, D. D'Arcangelis, E. Dolginova, C.A. Mannella, Molecular design of the voltage-dependent, anion-selective channel in the mitochondrial outer membrane, J. Struct. Biol. 114 (1995) 41–59.
[41] L. Shao, K.W. Kinnally, C.A. Mannella, Circular dichroism studies of the mitochondrial channel, VDAC, from *Neurospora crassa*, Biophys. J. 71 (1996) 778–786.
[42] M. Forte, H.R. Guy, C.A. Mannella, Molecular genetics of the VDAC ion channel: structural model and sequence analysis, J. Bioenerg. Biomembr. 19 (1987) 341–350.
[43] W.A. Summers, D.A. Court, Origami in outer membrane mimetics: correlating the first detailed images of refolded VDAC with over 20 years of biochemical data, Biochem. Cell Biol. 88 (2010) 425–438.
[44] S. Hiller, J. Abramson, C. Mannella, G. Wagner, K. Zeth, The 3D structures of VDAC represent a native conformation, Trends Biochem. Sci. 35 (2010) 514–521.
[45] K.I. Lee, H. Rui, R.W. Pastor, W. Im, Brownian dynamics simulations of ion transport through the VDAC, Biophys. J. 100 (2011) 611–619.
[46] H. Rui, K.I. Lee, R.W. Pastor, W. Im, Molecular dynamics studies of ion permeation in VDAC, Biophys. J. 100 (2011) 602–610.
[47] K.I. Lee, S. Jo, H. Rui, B. Egwolf, B. Roux, R.W. Pastor, W. Im, Web interface for Brownian dynamics simulation of ion transport and its applications to beta-barrel pores, J. Comput. Chem. 33 (2012) 331–339.
[48] O.P. Choudhary, R. Ujwal, W. Kowallis, R. Coalson, J. Abramson, M. Grabe, The electrostatics of VDAC: implications for selectivity and gating, J. Mol. Biol. 396 (2010) 580–592.
[49] S. Villinger, R. Briones, K. Giller, U. Zachariae, A. Lange, B.L. de Groot, C. Griesinger, S. Becker, M. Zweckstetter, Functional dynamics in the voltage-dependent anion channel, Proc. Natl. Acad. Sci. U. S. A. 107 (2010) 22546–22551.
[50] W. Im, B. Roux, Ion permeation and selectivity of OmpF porin: a theoretical study based on molecular dynamics, Brownian dynamics, and continuum electrodiffusion theory, J. Mol. Biol. 322 (2002) 851–869.
[51] T. Schirmer, P.S. Phale, Brownian dynamics simulation of ion flow through porin channels, J. Mol. Biol. 294 (1999) 1159–1167.
[52] J.C. Philipps, R. Braun, W. Wang, J. Gumbart, E. Tajkhorshid, E. Villa, C. Chipot, R.D. Skeel, L. Kale, K. Schulten, Scalable molecular dynamics with NAMD, J. Comput. Chem. 26 (2005) 1781–1802.
[53] W. Humphrey, A. Dalke, K. Schulten, VMD: visual molecular dynamics, J. Mol. Graph. 14 (1996) 33–38.
[54] S. Jo, T. Kim, V.G. Iyer, W. Im, CHARMM-GUI: a web-based graphical user interface for CHARMM, J. Comput. Chem. 29 (2008) 1859–1865.
[55] W. Im, S. Seefeld, B. Roux, A Grand Canonical Monte Carlo–Brownian dynamics algorithm for simulating ion channels, Biophys. J. 79 (2000) 788–801.
[56] J. Ryerse, M. Colombini, T. Hagerty, B. Nagel, T.T. Liu, Isolation and characterization of the mitochondrial channel, VDAC, from the insect *Heliothis virescens*, Biochim. Biophys. Acta 1327 (1997) 193–203.
[57] G. Yehezkel, S. Abu-Hamad, V. Shoshan-Barmatz, An N-terminal nucleotide-binding site in VDAC1: involvement in regulating mitochondrial function, J. Cell. Physiol. 212 (2007) 551–561.
[58] H. Troll, D. Malchow, A. Muller-Taubenberger, B. Humbel, F. Lottspeich, M. Ecke, G. Gerisch, A. Schmid, R. Benz, Purification, functional characterization, and cDNA sequencing of mitochondrial porin from *Dictyostelium discoideum*, J. Biol. Chem. 267 (1992) 21072–21079.
[59] O. Ludwig, P. De, V.F. Palmieri, R. Benz, Pore formation by the mitochondrial porin of rat brain in lipid bilayer membranes, Biochim. Biophys. Acta 860 (1986) 268–276.
[60] T.K. Rostovtseva, S.M. Bezrukov, ATP transport through a single mitochondrial channel, VDAC, studied by current fluctuation analysis, Biophys. J. 74 (1998) 2365–2373.
[61] H. Freitag, W. Neupert, R. Benz, Purification and characterisation of a pore protein of the outer mitochondrial membrane from *Neurospora crassa*, Eur. J. Biochem. 123 (1982) 629–636.
[62] O. Ludwig, J. Krause, R. Hay, R. Benz, Purification and characterization of the pore forming protein of yeast mitochondrial outer membrane, Eur. Biophys. J. 15 (1988) 269–276.
[63] E. Pavlov, S.M. Grigoriev, L.M. Dejean, C.L. Zweihorn, C.A. Mannella, K.W. Kinnally, The mitochondrial channel VDAC has a cation-selective open state, Biochim. Biophys. Acta 1710 (2005) 96–102.
[64] B. Popp, D.A. Court, R. Benz, W. Neupert, R. Lill, The role of the N and C termini of recombinant *Neurospora* mitochondrial porin in channel formation and voltage-dependent gating, J. Biol. Chem. 271 (1996) 13593–13599.